3-D VISCOELASTIC TIME-DOMAIN FINITE-DIFFERENCE SEISMIC MODELLING USING THE STAGGERED ADAMS-BASHFORTH TIME INTEGRATOR

T. Bohlen and F. Wittkamp

email: *thomas.bohlen@kit.edu*

keywords: *Wave propagation, numerical approximations and analysis, finite-differences, higher order, Adams-Bashforth*

ABSTRACT

We analyze the performance of a higher order accurate staggered viscoelastic time-domain Finite-Difference method, in which the staggered Adams-Bashforth (ABS) third-order and fourth-order accurate time integrators are used for temporal discretization. ABS is a multi-step method that uses previously calculated wavefields to increase the order of accuracy in time. The analysis shows that the numerical dispersion is much lower than that of the widely used second-order leapfrog method. Numerical dissipation is introduced by the ABS method which is significantly smaller for fourth-order than third-order accuarcy. In 1-D and 3-D simulation experiments we verify the convincing improvements of simulation accuracy of the fourth-order ABS method. In a realistic elastic 3-D scenario the computing time reduces by a factor of approximately 2.4, whereas the memory requirements increase by approximately a factor of 2.2. The ABS method thus provides an alternative strategy to increase the simulation accuracy in time by investing computer memory instead of computing time.

INTRODUCTION

Today, full wavefield seismic imaging and full waveform inversion require the efficient and accurate numerical simulation of seismic waves through complex earth models. For this purpose higher-order Finite-Difference (FD) methods are widely applied where the wave equation is discretized in both space and time. For the spatial derivatives different methods are available. For the time discretization, however, the second order FD leapfrog scheme is still common because of its easy implementation and no additional requirements of computer memory. Unfortunately, second order time integration is often inefficient as it requires a dense temporal sampling to achieve a sufficient accuracy. Higher order time stepping methods are thus desirable to save computation time. For this reason new techniques have been proposed that allow to increase the order of time discretization. They can be divided into low-storage methods and multi-step methods. Low-storage methods increase the temporal order without significantly increasing the memory requirements. Multi-step methods store the time history to increase the accuracy order.

An efficient and popular low-storage strategy today is the so-called Lax-Wendroff method which replaces high-order temporal derivatives in the Taylor series expansion by spatial derivatives using the wave equation (Dablain, 1986; Blanch and Robertsson, 1997; Schwartzkopff et al., 2004). However, in 2D and 3D media the Lax-Wendroff approach involves quite expensive calculations of high-order mixed spatial derivatives and thus leads to an increase of floating point operations on extended spatial stencils. Recently, Tan & Huang (2014) developed a shorter Lax-Wendroff-type stencil having only a few more grid points and floating point operations than the standard stencil. Another low-storage approach to increase the temporal accuracy is the predictor-corrector optimally accurate FD scheme of Geller & Takeuchi (1998). This scheme is essentially equivalent to a Lax-Wendroff scheme with fourth-order accuracy in both space and

time. Liu & Sen (2009) achieved higher order accuracy in time by minimizing the dispersion relations in the joint time-space domain. Their scheme yields higher order accuracy in 2D along eight spatial directions only. More recently, Liu & Sen (2013) improved this scheme to higher order accuracy for all spatial direction using a spatially extended rhombus-shaped stencil. Both the commonly applied Lax-Wendroff methods (Dablain, 1986; Tan and Huang, 2014) and the joint time-space discretization of Liu & Sen (2013) require spatially extended stencils which can lead to simulation errors in case of strong material discontinuities (Tan and Huang, 2014).

A memory intensive strategy to increase the temporal accuracy are multi-step methods (Hairer et al., 2006). In a multi-step method the history of the temporal evolution is stored to increase the order of the time integration. The classical way are Runge-Kutta methods that yield better accuracy for long-time simulations than the Lax-Wendroff schemes (Chen, 2007) but are limited to fourth order accuracy. Ghrist et al. (2000) compare two other multi-step methods, the staggered Adams-Bashforth (ABS) and the Backward Differentiation method (BDS) and show applications to the acoustic wave equation. Both have also been applied to Maxwell's equation for the 2-D TE mode (Xiao et al., 2007; Hwang and Ihm, 2006). These investigations show that for hyperbolic wave equations the numerical dispersion of both methods is similar but the stability restraint of the ABS method is much relaxed by approximately 33 per cent. Furthermore, the BDS method is stable for wave equation simulations up to fourth order only, whereas the ABS method is stable also for higher orders. The ABS method thus has considerable advantages compared to the BDS method.

In this work we therefore further evaluate the implementation of the ABS-method into 3-D staggered-grid viscoelastic FDTD schemes that are widely used for realistic and efficient seismic wavefield simulations. The ABS method was chosen because of the following advantages. (1) It has a relatively large region of stability. (2) The implementation is straightforward. (3) The time discretization is independent of the used spatial discretization scheme. (4) The increase of accuracy must be paid by the storage of the time evolution which is feasible today on modern parallel high performance computing (HPC) systems that are equipped with large memory capacity.

In this paper we first illustrate the implementation of the ABS-method for the 1-D acoustic wave equation. We analyze the numerical properties of the 1-D implementation with respect to accuracy, numerical dispersion and numerical dissipation. Afterwards we describe the implementation of the ABS-method for 3-D staggered grid velocity-stress time-domain viscoelastic simulation. We derive the stability limits and discuss the accuracy and computational requirements for 3-D simulations.

THEORY

For the sake of simplicity we first illustrate the staggered Adams-Bashforth method (ABS-method) using the 1-D acoustic wave equation in velocity-stress formulation

$$\begin{aligned} \frac{\partial p(x,t)}{\partial t} &= -\pi(x)\frac{\partial v(x,t)}{\partial x} \\ \frac{\partial v(x,t)}{\partial t} &= -\rho^{-1}(x)\frac{\partial p(x,t)}{\partial x} \end{aligned} \tag{1}$$

The wavefield variables are the pressure $p(x,t)$ and the particle velocity $v(x,t)$. The material is described by the P-wave modulus $\pi(x)$ and the mass density $\rho(x)$. For simplicity we omit the temporal (t) and spatial dependencies (x) in the following.

Using the conventional second order staggered grid approximation to the first order time derivative we obtain

$$\begin{aligned} \frac{p|^{n+1/2} - p|^{n-1/2}}{\triangle t} &= -\pi \frac{\partial v}{\partial x}\bigg|^{n} + \mathcal{O}(\triangle t^2) \\ \frac{v|^{n} - v|^{n-1}}{\triangle t} &= -\rho^{-1} \frac{\partial p}{\partial x}\bigg|^{(n-1/2)} + \mathcal{O}(\triangle t^2) \end{aligned} \tag{2}$$

M	a_0	a_1	a_2	a_3
2	1	0	0	0
3	25/24	-1/12	1/24	0
4	13/12	-5/24	1/6	-1/24

Table 1: Weights used for the summation of previous time levels in the Adams-Bashforth method (Ghrist et al., 2000).

This results in the conventional explicit second order accurate time-stepping (leapfrog) scheme

$$\begin{aligned} p|^{n+1/2} &= p|^{n-1/2} - \triangle t\pi \frac{\partial v}{\partial x}\Big|^{n} + \mathcal{O}(\triangle t^2) \\ v|^{n} &= v|^{n-1} - \triangle t\rho^{-1} \frac{\partial p}{\partial x}\Big|^{(n-1/2)} + \mathcal{O}(\triangle t^2) \end{aligned} \tag{3}$$

which requires no additional storage of the wavefield variables p and v.

With the ABS-method the order of the temporal integration can be increased by using previous time levels of the right hand sides of equation 2 (Ghrist et al., 2000). The ABS-method thus requires the storage of previous time levels of spatial derivatives of the pressure p and particle velocity v. The time update for the ABS-method thus reads

$$\begin{aligned} p|^{n+1/2} &= p|^{n-1/2} - \triangle t\pi \sum_{k=0}^{M-1} a_k \frac{\partial v}{\partial x}\Big|^{n-k} + \mathcal{O}(\triangle t^M) \\ v|^{n} &= v|^{n-1} - \triangle t\rho^{-1} \sum_{k=0}^{M-1} a_k \frac{\partial p}{\partial x}\Big|^{(n-1/2-k)} + \mathcal{O}(\triangle t^M) \end{aligned} \tag{4}$$

The weights for the time accuracy orders $M = 2, 3, 4$ are given in Table 1.

1-D SIMULATIONS

Seismograms

We first compare seismograms calculated with the 1-D ABS-method using equations 4 for different orders of accuracy in time (M). We use a 1-D homogeneous acoustic medium with a wave velocity of $c = 3500$ m/s and constant density of $\rho = 2000\,\mathrm{kg/m^3}$. The source signal is a Ricker signal with a center frequency of 600 Hz. We choose a large source-receiver distance of 120 dominant wavelength to emphasize the effects of numerical dispersion and numerical dissipation in the synthetic seismograms. The spatial derivatives are computed with high accuracy using a centered staggered FD stencil of 8th order accuracy. The spatial grid spacing is held constant at $\triangle x = 0.4$ m corresponding to approximately 14 grid points per dominant wavelength. Discrepancies to the analytical solution (time-shifted Ricker signal) are thus mainly caused by the chosen time step interval $\triangle t$ and the order of the temporal discretization ($M = 2, 3, 4$). The numerical results for Courant numbers $r = c\triangle t/\triangle x = 0.4, 0.2, 0.1$ and temporal orders of accuracy $M = 2, 3, 4$ are compared with the analytical solution in Figure 1. For a large Courant number of $r = 0.4$ (corresponding to a large time step interval) and second order approximation of the time derivative ($M = 2$) we can observe a large time dispersion error causing a leading phase with high amplitude (Figure 1, top-left). Figure 1 compares two ways to reduce this time discretization error. The conventional way is to stay with the given temporal order of accuracy (typically $M = 2$) and then reduce the time step interval, i.e. Courant number. The resulting waveforms are shown in the rows of Figure 1. Reducing the Courant number (time step interval) will increase the computation time proportional to $1/r$. The alternative way proposed in this study is to increase the order of the temporal discretization with the ABS-method which requires to store $M - 1$ previously calculated spatial derivates of wavefields. The resulting waveforms are shown in the columns of Figure 1.

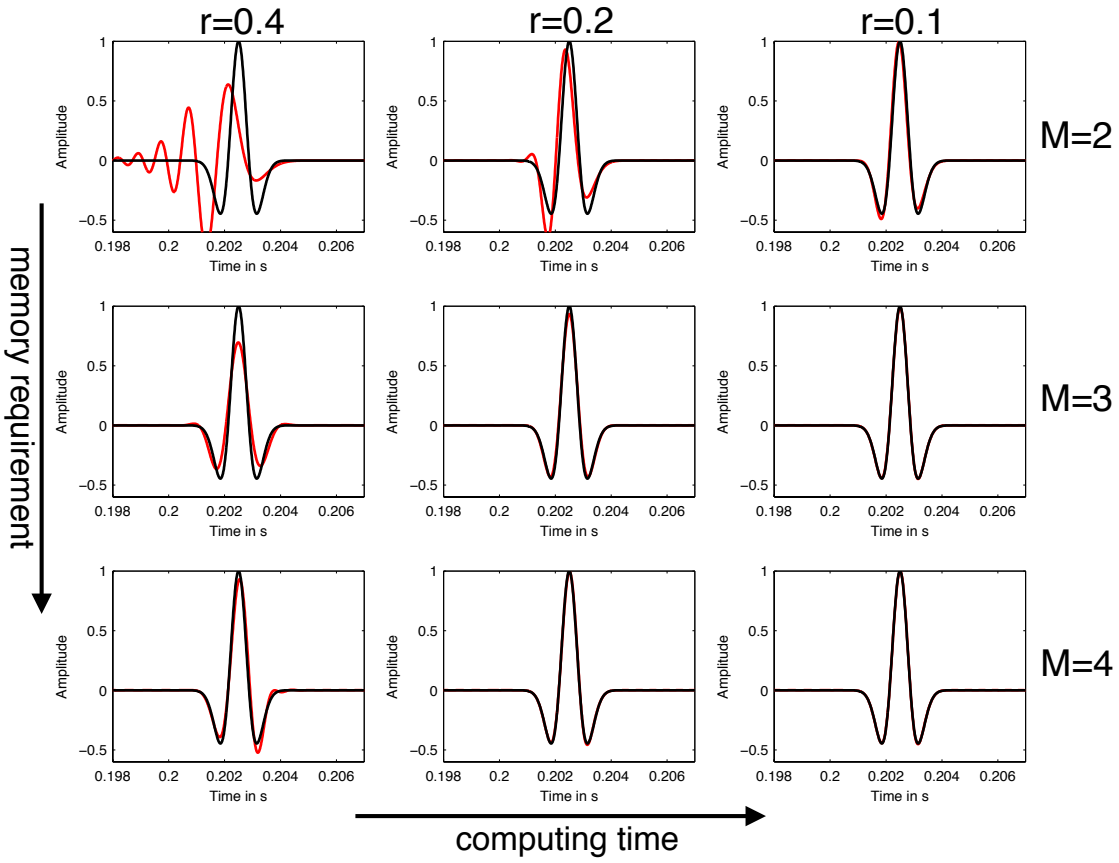

Figure 1: Seismograms (red lines) calculated for the 1-D case for different Courant numbers r and orders of accuracy M. $M = 2$ corresponds to the classical second order leapfrog scheme (equations 2). $M = 3, 4$ correspond to the multi-step ABS method (equations 4). The analytical solution is plotted as a black line.

Accuracy in 1-D

In Figure 1 we see that the simulation accuracy increases with decreasing Courant number and increasing order of accuracy. In order to quantify the corresponding numerical simulation error we calculated the normalized L2-misfit between the numerical and analytical solution for different Courant numbers and orders of accuracy $M = 2, 3, 4$. In Figure 2 we plot the normalized L2-misfit over the Courant number. As a secondary axis we plot the number of time steps $NT = T/\triangle t = Tc/(r\triangle x)$ that are required to yield the same propagation time of waves of $T = 0.24\,\mathrm{s}$. We can observe the expected higher order reduction of the simulation accuracy which reduces proportional to $\triangle t^M$ or NT^{-M}. For a given accuracy level of $E = 0.1\%$ (horizontal line in Figure 2) the required numbers of time steps are 39233, 13938, and 8704 for $M = 2, M = 3$ and $M = 4$, respectively. The number of time steps thus reduces to 36% and 22% when we increase the temporal order from $M = 2$ to 3 and 4, respectively (Figure 2). The ABS methods thus allows to significantly decrease the number of time steps to achieve a certain level of accuracy due to the higher order approximation of the time derivatives. This comes with an increase of the number of floating point operations per time step and additional memory requirements to store spatial derivative wave fields at previous time levels. The balance between these factors and the overall improvement of the performance will be discussed for realistic 3-D elastic simulations.

Numerical dispersion in 1-D

We performed a classical dispersion analysis by inserting a plain wave into the discrete scheme 4. The plain wave is described by

$$p = p_0 \cdot e^{i(kx+\omega t)} \text{ and } v = v_0 \cdot e^{i(kx+\omega t)} \tag{5}$$

which can be expressed in a discrete way as

$$p_j^n = p_0 \cdot e^{i(kj\Delta x+\omega n\Delta t)} \text{ and } v_j^n = v_0 \cdot e^{i(kj\Delta x+\omega n\Delta t)} \tag{6}$$

p_0 and v_0 are the amplitudes of the pressure p and particle velocity v. k denotes the wave number and ω is the circular frequency. j and n are the spatial and temporal indices, respectively. For the spatial derivatives in the ABS-method (equation 4) we use centered staggered grid approximations of the accuracy order N

$$\left.\frac{\partial v}{\partial x}\right|_j^n \approx \sum_{n=1}^{N/2} \beta_n \left(v_{j+(n-1/2)}^n - v_{j-(n-1/2)}^n \right) \tag{7}$$

where β_n are the FD weights than can be obtained by a Taylor series expansion. Inserting the discrete plane wave 6 into equation 7 yields

$$\left.\frac{\partial v}{\partial x}\right|_j^n \approx \frac{2iv_o z_j^n}{\triangle x} \sum_{n=1}^{N/2} \beta_n \sin\left(\frac{(2n-1)k\triangle x}{2}\right) = \frac{2iv_o z_j^n}{\triangle x} D(k\triangle x) \tag{8}$$

where we use the abbreviation $z_j^n = e^{(kj\Delta x+\omega n\Delta t)}$. The dispersion introduced by the spatial discretization is summarized in the factor

$$D(k\triangle x) = \sum_{n=1}^{N/2} \beta_n \sin\left(\frac{(2n-1)k\triangle x}{2}\right) \tag{9}$$

which we use in the following.

We now insert the discrete plane wave (eq. 6) into the update equations 4. The following dispersion relation ist obtained

$$\sin(\omega\triangle t/2) = rD(k\triangle x) \sum_{l=0}^{M-1} a_l e^{-i\omega l\triangle t} \tag{10}$$

from which we take the real part

$$\sin(\omega\triangle t/2) = rD(k\triangle x) \sum_{l=0}^{M-1} a_l \cos(\omega l\triangle t) \tag{11}$$

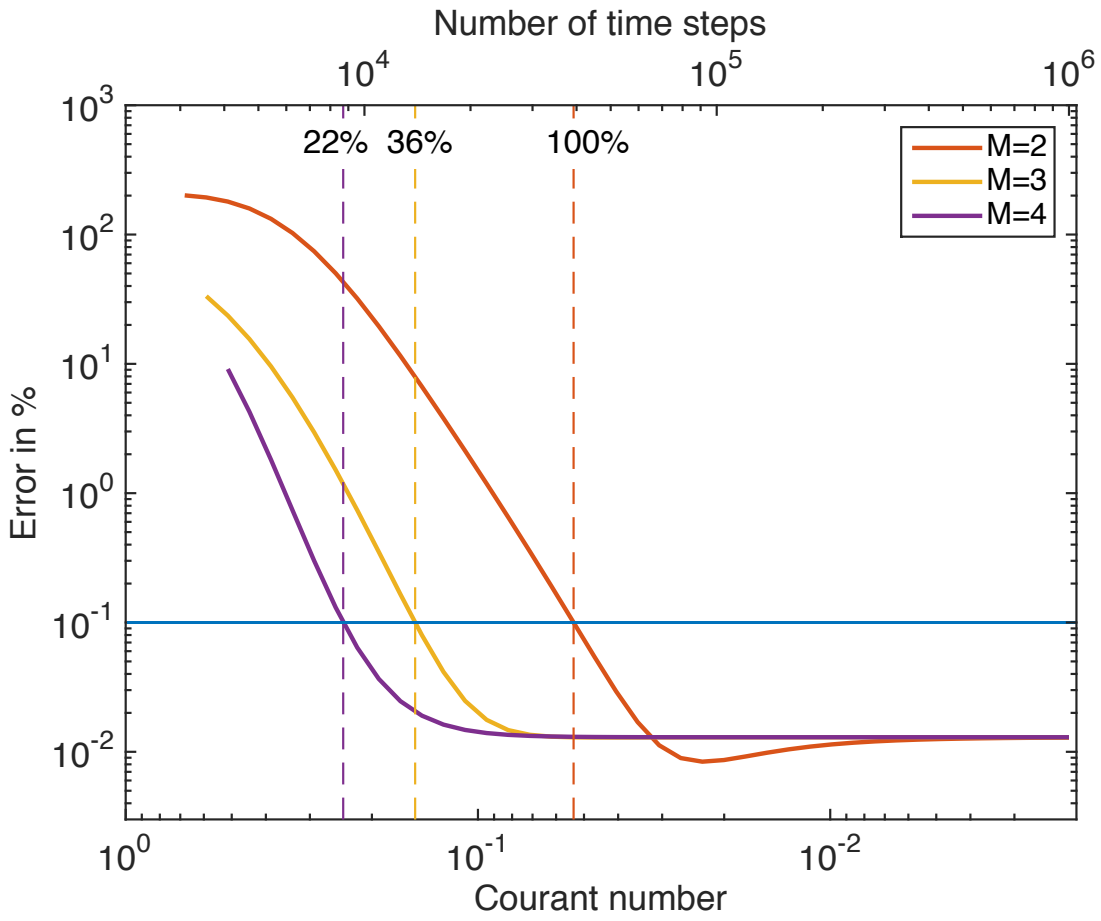

Figure 2: Relative error of 1-D simulations (Figure 1). The normalized L2 norm is plotted over the Courant number (bottom axis) and the number of time steps NT (top axis) required to yield the same propagation time. The temporal accuracy orders are $M = 2, 3, 4$. The spatial accuracy is fixed at order $N = 8$. The number of time steps to achieve a given accuracy of $E = 0.01\%$ (horizontal line) reduce to 36% and 22% for the temporal orders $M = 3$ and $M = 4$, respectively. For small Courant numbers (small time step intervals) the error converges to the fixed error of the spatial discretization.

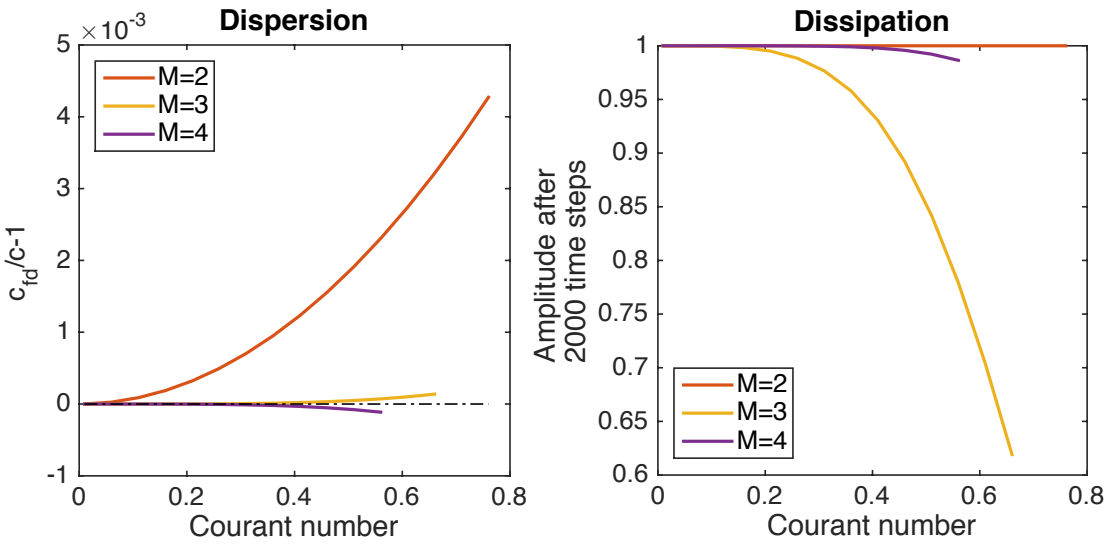

Figure 3: Numerical dispersion (left) and numerical dissipation (right) for the temporal orders $M = 2, 3, 4$ as a function of Courant number r. The curves are plotted up to the corresponding stability limits. The accuracy order of the staggered grid spatial derivatives is $N = 8$ (equation 7). The dominant wavelength is discretized with approximately 14 grid points.

to calculate the ratio between the numerical wave velocity $c_{\text{fd}} = \frac{\omega}{k}$ and the model velocity c

$$\frac{c_{\text{fd}}}{c} = \frac{\frac{\omega}{k}}{c} = \frac{\frac{\omega}{k}}{\frac{r \cdot \Delta x}{\Delta t}} = \frac{\omega \Delta t}{k \cdot \Delta x \cdot r} \tag{12}$$

Substitution equation 12 into equation 11 yields the implicit dispersion relation

$$\sin(\phi) = rD(k\triangle x) \sum_{l=0}^{M-1} a_l \cos(\phi) \text{ with } \phi = \frac{1}{2} \frac{c_{\text{fd}}}{c} kr\triangle x \tag{13}$$

Here the spatial dispersion factor $D(k\triangle x)$ can be nicely separated. It is thus straightforward to calculate the numerical dispersion of the ABS-method for other methods of approximations of spatial derivatives.

The relative numerical propagation velocity $\frac{c_{\text{fd}}}{c} - 1$ as a function of the Courant number r is obtained by numerically solving equation 13. The results are shown in Figure 3 (right). We see a significant reduction of the numerical time dispersion error when increasing the temporal order of accuracy from $M = 2$ to 3 or 4. The magnitude of numerical dispersion of orders $M = 3$ and $M = 4$ is comparable. For $M = 3$ we obtain faster numerical velocities, whereas the numerical velocities for $M = 4$ are smaller than the model velocity c.

Numerical dissipation in 1-D

In contrast to the common leapfrog scheme ($M = 2$), the ABS method ($M > 2$) exhibits numerical amplitude loss with propagation distance called numerical dissipation. In order to quantify the numerical dissipation we introduce an amplification factor g (Fei and Xiaohong, 2006).

$$p_j^n = p_0 \cdot g^n \cdot e^{i \cdot j \cdot k \Delta x}, \tag{14}$$

$$v_j^n = v_0 \cdot g^n \cdot e^{i \cdot j \cdot k \Delta x} = -\frac{c}{\pi} \cdot p_0 \cdot g^n \cdot e^{i \cdot j \cdot k \Delta x} \tag{15}$$

If we insert this ansatz into the staggered grid approximation of spatial derivatives (equation 7) we obtain

$$\left.\frac{\partial v}{\partial x}\right|_j^n \approx \frac{2iv_o e^{ikj\triangle x}}{\triangle x} D(k\triangle x) g^n \tag{16}$$

When inserting equations 16 and 15 into the update scheme of the pressure (equation 4) we obtain the following characteristic polynomial in g

$$0 = g^{\frac{1}{2}} - g^{-\frac{1}{2}} - 2irD(k\triangle x) \sum_{l=0}^{M-1} a_l g^{-l} \tag{17}$$

We used the modulus of the smallest root of this characteristic polynomial to calculate the amplitude of wavefield after 2000 time steps as a function of the Courant number r. The results are shown in Figure 3 (left). The leapfrog scheme ($M = 2$) is free of dissipation. The ABS-method of temporal order $M = 3$ suffers from quite significant dissipation, whereas the dissipation caused by the fourth order approximation ($M = 4$) is much smaller. The strong dissipation for $M = 3$ is also clearly visible in Figure 1 for a large Courant number of $r = 0.4$. $M = 3$ thus may lead to an underestimation of simulated amplitudes especially for long times of wave propagation.

3-D IMPLEMENTATION

3-D viscoelastic wave equations

We implemented the ABS-method into a 3-D viscoelastic staggered grid velocity-stress time-domain Finite-Difference (FDTD) simulation code (Bohlen, 2002). The underlying first order system of partial differential equations consists of the the stress-strain relation for a generalized standard linear solid

$$\begin{aligned}
\dot{\sigma}_{ij} &= \left(\pi\left(1 + L\tau^p\right) - 2\mu\left(1 + L\tau^s\right)\right) T \\
&\quad + 2\mu\left(1 + L\tau^s\right) \frac{\partial v_i}{\partial x_j} + \sum_{l=1}^{L} r_{ijl} \quad \text{if } i = j \quad , \\
\dot{\sigma}_{ij} &= \mu\left(1 + L\tau^s\right) \dot{\epsilon_{ij}} + \sum_{l=1}^{L} r_{ijl} \quad \text{if } i \neq j \quad ,
\end{aligned} \tag{18}$$

the equations for the L memory variables ($l = 1, ..., L$)

$$\begin{aligned}
\dot{r}_{ijl} &= -\frac{1}{\tau_{\sigma l}} \left\{ \left(\pi\tau^p - 2\mu\tau^s\right) T + 2 \frac{\partial v_i}{\partial x_j} \mu\tau^s + r_{ijl} \right\} \text{if } i = j \quad , \\
\dot{r}_{ijl} &= -\frac{1}{\tau_{\sigma l}} \left\{ \mu\tau^s \dot{\epsilon_{ij}} + r_{ijl} \right\} \quad \text{if } i \neq j \quad ,
\end{aligned} \tag{19}$$

and the equations of momentum conservation

$$\varrho \frac{\partial v_i}{\partial t} = \frac{\partial \sigma_{ij}}{\partial x_j} + f_i \quad . \tag{20}$$

where $\dot{\epsilon_{ij}} = \left(\frac{\partial v_i}{\partial x_j} + \frac{\partial v_j}{\partial x_i}\right)$ denotes the first time derivative of the deformation tensor and $T = trace\left\{\dot{\epsilon_{ij}}\right\}$ the cubic dilatation. The meaning of the remaining symbols is as follows:

σ_{ij}	denotes the ijth component of the stress tensor (i,$j = 1, 2, 3$),
v_i	denote the components of the particle velocities,
x_i	indicate the three spatial directions (x,y,z),
r_{ijl}	are the L memory variables (l = 1,...,L),
f_i	denotes the components of external body force,
$\tau_{\sigma l}$	are the L stress relaxation times for both P- and S-waves,
τ^p, τ^s	define the level of attenuation for P- and S-waves, respectively,
ϱ	is the mass density,
π and μ	are the moduli for P- and S-waves, respectively.

A derivation of these equations can be found for example in Robertsson et al. (1994). Following Blanch et al. (1995), we use the variable τ in the wave equation formulation.

3-D scheme

As described in the theory section the ABS-method is essentially a weighted summation over previous time levels of each right hand side (RHS) of equations 18, 19, and 20. The method is thus independent of the numerical procedure used to calculate spatial derivatives. In the following we therefore denote the time discretization only. We discretize the time evolution on a staggered grid where full time levels are denoted by n and intermediate time levels by $n \pm 1/2$.

If we apply the staggered time discretization and take weighted summations of each RHS of the form $\sum_{k=0}^{M-1} a_k (\text{RHS})|^{n-k}$ we obtain the following explicit velocity stress update scheme that has a time accuracy of the order M.

$$
\begin{aligned}
\sigma_{ij}|^{n+1/2} &= \sigma_{ij}|^{n-1/2} \\
&\quad + \triangle t \left(\pi \left(1 + L\tau^p\right) - 2\mu \left(1 + L\tau^s\right)\right) \sum_{k=0}^{M-1} a_k T|^{n-k} \\
&\quad + 2\triangle t \mu \left(1 + L\tau^s\right) \sum_{k=0}^{M-1} a_k \frac{\partial v_i}{\partial x_j} \Big|^{n-k} \\
&\quad + \frac{\triangle t}{2} \sum_{k=0}^{M-1} a_k \sum_{l=1}^{L} \left(r_{ijl}|^{n+1/2-k} + r_{ijl}|^{n-1/2-k} \right) \\
&\quad \text{if } i = j \quad , \\
\sigma_{ij}|^{n+1/2} &= \sigma_{ij}|^{n-1/2} + \triangle t \mu \left(1 + L\tau^s\right) \sum_{k=0}^{M-1} a_k \dot{\epsilon_{ij}}|^{n-k} \\
&\quad + \frac{\triangle t}{2} \sum_{k=0}^{M-1} a_k \sum_{l=1}^{L} \left(r_{ijl}|^{n+1/2-k} + r_{ijl}|^{n-1/2-k} \right) \\
&\quad \text{if } i \neq j \quad ,
\end{aligned}
\tag{21}
$$

$$
\begin{aligned}
r_{ijl}|^{n+1/2} &= \left(1 + \frac{a_0 \triangle t}{2\tau_{\sigma l}}\right)^{-1} \left[-\frac{\triangle t}{\tau_{\sigma l}} \left(\pi \tau^p - 2\mu\tau^s\right) \sum_{k=0}^{M-1} a_k T|^{n-k} \right. \\
&\quad + \frac{\triangle t 2\mu\tau^s}{\tau_{\sigma l}} \sum_{k=0}^{M-1} a_k \frac{\partial v_i}{\partial x_j} \Big|^{n-k} \\
&\quad + \left(1 - \frac{a_0 \triangle t}{2\tau_{\sigma l}}\right) r_{ijl}|^{n-1/2} \\
&\quad \left. - \frac{\triangle t}{2\tau_{\sigma l}} \sum_{k=1}^{M-1} a_k \sum_{l=1}^{L} \left(r_{ijl}|^{n+1/2-k} + r_{ijl}|^{n-1/2-k} \right) \right] \\
&\quad \text{if } i = j \quad , \\
r_{ijl}|^{n+1/2} &= \left(1 + \frac{a_0 \triangle t}{2\tau_{\sigma l}}\right)^{-1} \left[-\frac{\triangle t}{\tau_{\sigma l}} \mu \tau^s \sum_{k=0}^{M-1} a_k \dot{\epsilon_{ij}}|^{n-k} \right. \\
&\quad + \left(1 - \frac{a_0 \triangle t}{2\tau_{\sigma l}}\right) r_{ijl}|^{n-1/2} \\
&\quad \left. - \frac{\triangle t}{2\tau_{\sigma l}} \sum_{k=1}^{M-1} a_k \sum_{l=1}^{L} \left(r_{ijl}|^{n+1/2-k} + r_{ijl}|^{n-1/2-k} \right) \right] \\
&\quad \text{if } i \neq j \quad ,
\end{aligned}
\tag{22}
$$

$$v_i|^{n+1} = v_i|^n + \frac{\triangle t}{\varrho} \sum_{k=0}^{M-1} a_k \frac{\partial \sigma_{ij}}{\partial x_j} \Big|^{n+1/2-k} \tag{23}$$

3-D stability analysis

We performed the von Neumann stability analysis to find the stability limits for the viscoelastic update scheme presented in equations 21-23. In the stability analysis we use the update equation for the x-component of particle velocity only. Numerical simulations, however, show that the obtained stability limits hold also for the full 3-D elastic update scheme.

If we insert the discrete eigenmodes

$$\begin{aligned} v_x|^n &= v_{x0} \cdot g^n \cdot e^{i(k_x l \triangle x + k_y m \triangle y + k_z p \triangle z)} \\ \sigma_{xi}|^n &= \sigma_{xi0} \cdot g^n \cdot e^{i(k_x l \triangle x + k_y m \triangle y + k_z p \triangle z)}, i = x, y, z \end{aligned} \tag{24}$$

into the update equation for the horizontal particle velocity

$$v_x|^{n+1} = v_i|^n + \frac{\triangle t}{\varrho} \sum_{k=0}^{M-1} a_k \frac{\partial \sigma_{xj}}{\partial x_j} \Big|^{n+1/2-k} \tag{25}$$

we obtain the following polynomial for the amplification factor g

$$g^1 = g^0 - 2i\sqrt{3} \cdot D(k\triangle h) \cdot r \sum_{k=0}^{M-1} a_k g^{1/2-k} \tag{26}$$

In the derivation of equation 26 we assumed an equidistant grid with spacing $\triangle h = \triangle x = \triangle y = \triangle z$. We further assumed that the waves propagate in an homogeneous medium ($\varrho = \text{const}$, $c = \text{const}$) along the diagonals of each grid cell. We can thus write for the corresponding wave number $k = \sqrt{k_x^2 + k_y^2 + k_z^2} = \sqrt{3}k_x$. The amplitudes of the inserted eigenmodes are related via $\varrho c\sqrt{3}v_{x0} = \sigma_{xx0} + \sigma_{xy0} + \sigma_{xz0}$. This relation is obtained by inserting a plane wave into the equation of motion. The dispersion due to the spatial discretization is hidden in the factor $D(k\triangle h)$. Rearranging equation 26 to the Courant number r yields

$$r = \frac{-i\left(g^1 - g^0\right)}{2 \cdot \sqrt{3} \cdot D(k\triangle h) \cdot \sum_{k=0}^{M-1} a_k \cdot g^{\frac{1}{2}-k}} \tag{27}$$

The criterium for stability is that the inserted eigenmodes are bound. This is fulfilled if $|g| \leq 1$. This means that roots of the characteristic polynominal must lie inside or on the unity circle $e^{i\Theta}$ (Fei and Xiaohong, 2006). Courant numbers r_{max} for which $g = e^{i\Theta}$ thus define the stability limits.

$$r_{max} = \text{MAX}\left| \frac{-i\left(e^{i\cdot 1\cdot\Theta} - e^{-i\cdot 0\cdot\Theta}\right)}{2 \cdot \sqrt{3} \cdot D(\pi) \cdot \sum_{k=0}^{M-1} a_k \cdot e^{i\cdot\Theta\cdot(\frac{1}{2}-k)}} \right| \tag{28}$$

For the spatial dispersion factor we insert the dispersion $D(\pi)$ at the Nyquist wave number $k\triangle h = \pi$. We assumed symmetric staggered Taylor series approximation of the order N for the spatial derivatives (equation 7). In this case the factor becomes $D(\pi) = \sum_{n=1}^{N/2} \beta_n$. We solved equation 28 numerically. The obtained stability limits r_{max} are listed in table 2 for different orders of accuracy used for the spatial and temporal approximations. The stability limits presented in Table 2 have been verified by 3-D elastic simulations. With increasing spatial and temporal order r_{max} is decreasing, i.e. the region of stability is getting more restricted and smaller time step intervals are required for stable simulations.

	$M=2$	$M=3$	$M=4$
$N=2$	0.577	0.494	0.384
$N=4$	0.494	0.424	0.329
$N=6$	0.464	0.398	0.309
$N=8$	0.448	0.384	0.299
$N=10$	0.438	0.375	0.292

Table 2: Stability limits for 3-D elastic/viscoelastic FDTD simulations using equations 21-23. The maximum Courant-Friedrichs-Lewy number r_{max} (equation 28) is given for different accuracy orders of the temporal (M) and spatial (N) approximations.

Accuracy in 3-D

We analyzed the accuracy of the 3-D elastic update scheme which is obtained by setting $L = 0$ in the corresponding viscoelastic equations 21-23. We used the same set-up as in the accuracy analysis for the 1-D case presented before. We compared the synthetic seismograms with an analytical solution for an explosive point source in a homogeneous full space. The elastic model parameters are $v_p = 3500$ m/s and $v_s = 2000$ m/s for the P- and S-velocities, respectively, and $\varrho = 2000$ kg/m^3 for the density. The explosive point source generates a Ricker signal with a dominant frequency of 600 Hz. We analyze the accuracy of the direct P-wave in a distance of 180 m corresponding to 30 dominant wavelength. The size of the model grid is 800x400x400 grid points. The direct P-wave is spatially sampled with approximately 14 grid points per dominant wavelength. The influence of numerical dispersion due to the discretization in space is small because of the chosen high spatial accuracy order of $N = 8$. The simulations are performed on 80 cores on a small-scale shared memory cluster with the software SOFI3D (Bohlen, 2002).

As a measure of accuracy we again use the normalized L2-norm between the numerical and analytical seismograms which only contain the direct P-wave. The results are shown in Figure 4 (left). The L2-error reduces with increasing number of time steps $NT = T/\triangle t$ because of the decreasing time step interval $\triangle t$. (The wave propagation time $T = 0.07$ s is held constant). At higher orders of the time accuracy (M) the error reduces more rapidly proportional to $\triangle t^M$. The observed overall behavior of the convergence of accuracy in the 3-D elastic case (Figure 4, left) is quite similar to the convergence obtained for the 1-D scheme shown in Figure 2. This indicates that the numerical dispersion and dissipation properties derived for the 1-D case are also applicable to P-waves in 3-D media.

In Figure 4 (left) we see see that we can reduce the number of time steps that are required to achieve a certain level of accuracy by increasing the temporal accuracy order M. For a given error level of $E = 0.1\%$ the required number of time steps reduce to approximately 43% and 29% when increasing the temporal order from $M = 2$ to $M = 3$ and $M = 4$, respectively. The corresponding run times decrease less significant because the number of floating point operations also increase with M. The observed relation between the number of time steps and the total run time is plotted in Figure 4 (right). The computational requirements are also summarized in Table 3. We see that the corresponding run times reduce only to 58% and 42% for $M = 3$ and $M = 4$, respectively, which is still a substantial improvement. The downside of these significant run time savings is the boost of the memory requirements which increase to 174% and 220% (Table 3). Interestingly, the factor for the run time reduction and the increase factor for memory are quite similar to the same accuracy order M.

CONCLUSIONS

The ABS method is an efficient way to increase the time accuracy of explicit time-stepping simulation codes. The implementation is straightforward as it is independent of the method used to calculate the spatial derivatives. The method is thus directly applicable also to e.g. pseudo-spectral or discontinuous Galerkin methods which also apply explicit time stepping to advance in time. The ABS method does not require much additional floating point operations but the additional storage of $M-1$ perviously calculated time-levels of spatial derivative wave fields. It thus opens an alternative way to improve the time accuracy by investing computer memory instead of computing time. This seems to be affordable on modern parallel

	$M = 2$	$M = 3$	$M = 4$
Run time	4349 s	2505 s	1833 s
	100%	**58%**	**42%**
Time steps	8133	3505	2350
	100%	**43%**	**29%**
Total memory	19.9 GB	34.7 GB	43.8 GB
	100%	**174%**	**220%**
Error	0.10013%	0.10014%	0.10013%

Table 3: Comparison of computational demands for 3-D elastic FDTD simulations with the ABS time integrator of accuracy M to achieve the same level of accuracy. The required run time and number of time steps decrease with M. At the same time the total requirements of memory increase by approximately the same factor due to the required storage of previously calculated wavefields.

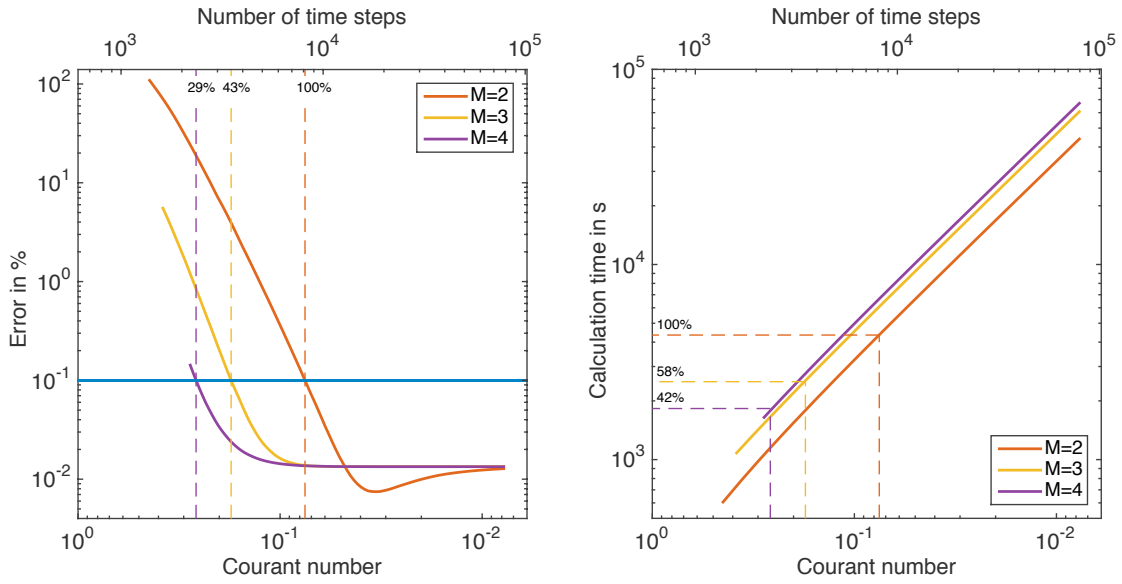

Figure 4: Left: Relative error of 3-D elastic simulations. The normalized L2 norm is plotted over the Courant number (bottom axis) and the number of time steps NT (top axis). The temporal accuracy orders are $M = 2, 3, 4$. The spatial accuracy is fixed at order $N = 8$. The number of time steps to achieve a given accuracy of $E = 0.1\%$ (horizontal line) reduce to 43% and 29% for the temporal orders $M = 3$ and $M = 4$, respectively. For large NT (small time step intervals) the error converges to the fixed error of the spatial discretization. Right: The required run time of the program as a function of the Courant number and number of time steps. The total run time to achieve an accuracy level of $E = 0.1\%$ reduces to 58% and 42% for the temporal orders of $M = 3$ and $M = 4$, respectively.

high performance computing systems that are equipped with large memory capacities which are generally not fully exploited by the conventional low-storage second order leap-frog schemes.

ACKNOWLEDGMENTS

This work was kindly supported by the sponsors of the *Wave Inversion Technology (WIT) Consortium*. We thank Marlis Hochbruck (KIT) and Christian Wieners (KIT) for helpful discussions regarding multi-step methods. We gratefully acknowledge financial support by the Deutsche Forschungsgemeinschaft (DFG) through CRC 1173. The simulations were performed on the computational resource Institutscluster II funded by participating KIT institutes and the DFG. The authors gratefully acknowledge the computing time granted on the supercomputer JUROPA at Juelich Supercomputing Centre (JSC).

REFERENCES

Blanch, J. and Robertsson, J. (1997). A modified lax-wendroff correction for wave propagation in media described by zener elements. *Geophysical Journal International*, 131(2):381–386.

Blanch, J., Robertsson, J., and Symes, W. (1995). Modeling of a constant Q: Methodology and algorithm for an efficient and optimally inexpensive viscoelastic technique. *Geophysics*, 60(1):176–184.

Bohlen, T. (2002). Parallel 3-D viscoelastic finite-difference seismic modelling. *Computers & Geosciences*, 28(8):887–899.

Chen, J.-B. (2007). High-order time discretizations in seismic modeling. *Geophysics*, 72(5):SM115–SM122.

Dablain, M. (1986). The application of high-order differencing to the scalar wave equation. *Geophysics*, 51:54–66.

Fei, X. and Xiaohong, T. (2006). Stability and numerical dispersion analysis of a fourth-order accurate fdtd method. *Antennas and Propagation, IEEE Transactions on*, 54(9):2525–2530.

Geller, R. J. and Takeuchi, N. (1998). Optimally accurate second-order time-domain finite difference scheme for the elastic equation of motion: one-dimensional cases. *Geophysical Journal International*, 135(1):48–62.

Ghrist, M., Fornberg, B., and Driscoll, T. A. (2000). Staggered time integrators for wave equations. *SIAM Journal on Numerical Analysis*, 38(3):718–741.

Hairer, E., Nørsett, S., and Wanner, G. (2006). *Solving ordinary differential equations*. Springer.

Hwang, K.-P. and Ihm, J.-Y. (2006). A stable fourth-order fdtd method for modeling electrically long dielectric waveguides. *Lightwave Technology, Journal of*, 24(2):1048–1056.

Liu, Y. and Sen, M. K. (2009). A new time–space domain high-order finite-difference method for the acoustic wave equation. *Journal of computational Physics*, 228(23):8779–8806.

Liu, Y. and Sen, M. K. (2013). Time-space domain dispersion-relation-based finite-difference method with arbitrary even-order accuracy for the 2d acoustic wave equation. *J. Comput. Phys.*, 232(1):327–345.

Robertsson, J., Blanch, J., and Symes, W. (1994). Viscoelastic finite-difference modeling. *Geophysics*, 59(9):1444–1456.

Schwartzkopff, T., Dumbser, M., and Munz, C.-D. (2004). Fast high order ader schemes for linear hyperbolic equations. *Journal of Computational Physics*, 197(2):532–539.

Tan, S. and Huang, L. (2014). An efficient finite-difference method with high-order accuracy in both time and space domains for modelling scalar-wave propagation. *Geophysical Journal International*.

Xiao, F., Tang, X., and Wang, L. (2007). An explicit fourth-order accurate fdtd method based on the staggered adams-bashforth time integrator. *Microwave and Optical Technology Letters*, 49(4):910–912.